


[View Journal Online](#)
[View Article Online](#)

Synthesis and detailed characterization of a newly synthesized chalcone, 3-(2,5-dimethoxyphenyl)-1-(naphthalen-2-yl)prop-2-en-1-one

Madhu Kumar Dogganal Jayappa ¹, Prabhuswamy Akhileshwari ²,
 Mandayam Anandalwar Sridhar ^{2,*}, Lohith Tumakuru Nagarajappa ²,
 Shivegowda Nagaraju ³, Subrayachar Raghavendra ³ and Manasa Dogganal Jayappa ⁴

¹ Faculty of Pharmacy, Ramaiah Institute of Applied Sciences, Bengaluru 560 054, India
madhuvandj@gmail.com (M.K.D.J.)

² Department of Studies in Physics, Manasagangotri, University of Mysore, Mysuru 570 006, India
akhila@uomphysics.net (P.A.), mas@physics.uni-mysore.ac.in (M.A.S.), lohith@uomphysics.net (L.T.N.)

³ Department of Engineering Physics, Adichunchanagiri Institute of Technology, Chikkamagaluru 577 102, India
nagubss@gmail.com (S.N.), raghuphotonics@gmail.com (S.R.)

⁴ Department of Applied Botany, Davanagere University, Davanagere 577 007, India
manasad310@gmail.com (M.D.J.)

* Corresponding author at: Department of Studies in Physics, Manasagangotri, University of Mysore, Mysuru 570 006, India.
 e-mail: mas@physics.uni-mysore.ac.in (M.A. Sridhar).

RESEARCH ARTICLE

ABSTRACT



doi 10.5155/eurjchem.12.1.69-76.2067

Received: 12 January 2021
 Received in revised form: 11 February 2021
 Accepted: 18 February 2021
 Published online: 31 March 2021
 Printed: 31 March 2021

KEYWORDS

Chalcone
 Single crystal structure
 Reduced density gradient
 Hirshfeld surface analysis
 Frontier molecular orbitals
 Molecular electrostatic potential

Chalcones are the main component of some natural compounds. The title compound, 3-(2,5-dimethoxyphenyl)-1-(naphthalen-2-yl)prop-2-en-1-one, was synthesized and characterized. The compound (C₂₁H₁₈O₃) crystallizes in the triclinic system with the space group of *P*-1 (no. 2), *a* = 7.7705(4) Å, *b* = 10.2634(6) Å, *c* = 11.2487(6) Å, α = 79.655(5)°, β = 81.500(5)°, γ = 68.039(5)°, *V* = 815.28(9) Å³, *Z* = 2, *T* = 293(2) K, μ (MoK α) = 0.086 mm⁻¹, *D*_{calc} = 1.297 g/cm³, 9126 reflections measured (4.318° ≤ 2 θ ≤ 52.728°), 3302 unique (*R*_{int} = 0.0466, *R*_{sigma} = 0.0528) which were used in all calculations. The final *R*₁ was 0.0568 (*I* > 2 σ (*I*)) and *wR*₂ was 0.1667 (all data). The crystal structure is stabilized by both short C-H...O inter- and intra-molecular interactions. In addition, the crystal structure is reinforced by π - π interactions. Hirshfeld surface analysis confirmed the presence of C-H...O intermolecular interactions. The two-dimensional fingerprint plots are used to visualize the individual interactions present in the molecule. DFT calculations were performed to know the energy levels of the frontier molecular orbitals (HOMO-LUMO). The energy gap between the frontier molecular orbitals shows the kinetic stability of the molecule. The chemical reactive sites are observed by generating MEP surface. Non-covalent interactions (NCIs) are analyzed using reduced density gradient (RDG) analysis.

Cite this: *Eur. J. Chem.* 2021, 12(1), 69-76

Journal website: www.eurjchem.com

1. Introduction

Chalcone is an aromatic ketone that forms the central core for a variety of important biological compounds [1,2]. The term "chalcone" is used to describe compounds with the 1,3-diphenylprop-2-en-1-one framework. They are naturally occurring compounds found in various plant species like *Angelica*, *Glycyrrhiza*, *Humulus*, and *Scutellaria*, which are widely used in folk remedies [3-6]. The products used daily as fruits, spices, tea, vegetables, and soybean-based food items contain derivatives of chalcone [7]. Chalcones are intermediates in the biosynthesis of flavonoids, substances which are widespread in compounds, exhibiting an array of biological activities [8]. The chalcone derivatives have attracted increasing attention due to their diverse biological activities such as anti-malarial, anticancer, anti-inflammatory, antioxidant, anti-

protozoal, antiulcer, and antibacterial [9-11]. Some biological compounds with embedding chalcone core are shown in Figure 1. They also exhibit many pharmacological activities such as cytotoxic agents, antiviral, anesthetics, mydriatics, etc. [12]. In view of the varied biological and pharmacological applications, the title compound was synthesized. The single crystal X-ray diffraction studies revealed the structure parameters. Quantum chemical computations were done to know the properties of the molecule.

2. Experimental

2.1. Synthesis of 3-(2,5-dimethoxyphenyl)-1-(naphthalen-2-yl)prop-2-en-1-one

A mixture of equimolar amount 1-(naphthalen-2-yl)ethenone (0.1 mol) was dissolved in methanol followed by

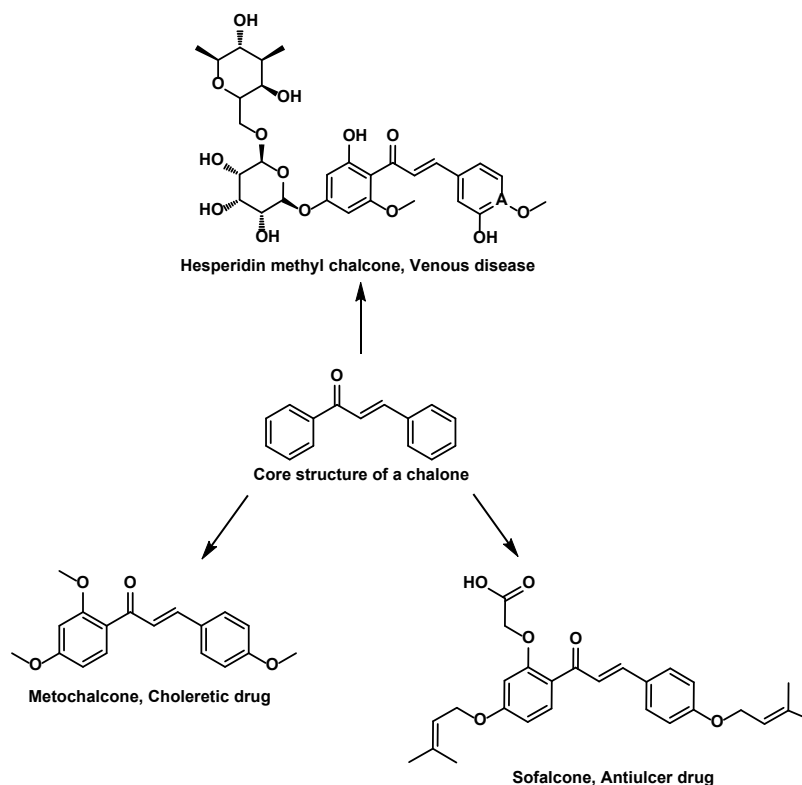


Figure 1. Some biological compounds with embedding chalcone core.

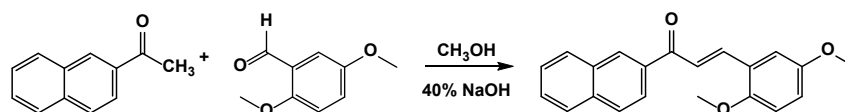


Figure 2. Synthesis of 3-(2,5-dimethoxyphenyl)-1-(naphthalen-2-yl)prop-2-en-1-one.

addition of 10 mL of 40% sodium hydroxide (NaOH) solution under stirring and a solution of 2,5-dimethoxy benzaldehyde (0.1 mol) in methanol was added. Stirring was continued for 6-8 hours [13]. The completion of the reaction was monitored by thin layer liquid chromatography (TLC) method and the reaction mixture was cooled and poured into ice-cold water. The precipitate was filtered, washed, and recrystallized from hot ethanol and little dimethylformamide (DMF). The crystals obtained were used for single crystal X-ray diffraction studies. The reaction scheme for the synthesized compound is shown in Figure 2.

2.2. X-ray diffraction analysis

A white colored rectangular block of the crystal with approximate dimensions of $0.31 \times 0.24 \times 0.23$ mm was selected for the X-ray diffraction study. The X-ray intensity data for the compound were collected at the temperature of 293(2) K on a Rigaku Saturn 724 diffractometer using graphite monochromated MoK α radiation. All frames were indexed using the triclinic system in the space group *P*-1. The complete data set was processed using CrystalClear [14]. The structure was solved by direct methods and refined by full-matrix least-squares on F^2 using SHELXS and SHELXL [15] programs, respectively. The ORTEP [16] and packing diagrams were generated using the MERCURY [17] software. All non-hydrogen atoms were revealed in the first Fourier map itself. The hydrogen atoms were positioned geometrically and were allowed to ride on their parent atoms. 219 parameters were refined with 3302

unique reflections. The final residual value converged to $R = 0.0568$ with a goodness of fit 1.050.

3. Results and discussion

3.1 Molecular structure description

The unit cell parameters are $a = 7.7705(4)$ Å, $b = 10.2634(6)$ Å, $c = 11.2487(6)$ Å, $\alpha = 79.655(5)^\circ$, $\beta = 81.500(5)^\circ$, $\gamma = 68.039(5)^\circ$ with $Z = 2$. The asymmetric unit contains one molecule. The details of the crystal structure and data refinement are given in Table 1. The bond lengths and bond angles are in good agreement with the standard values [18]. The list of selected bond lengths, bond angles, and torsion angles are given in Tables 2-3, respectively. The ORTEP of the molecule with thermal ellipsoids drawn at 50% probability is shown in Figure 3.

The structure consists of 2,5-dimethoxyphenyl and a naphthalene moiety, connected via a propenone chain. The rings in the molecule are sp^2 hybridized. The dihedral angle between the phenyl ring (C14-C15-C16-C17-C18-C19) and the naphthalene ring (C1-C2-C3-C4-C5-C6-7-C8-C9-C10) bridged by propenone is $78.83(9)^\circ$. The naphthalene ring is nearly planar with a maximum rms deviation of $0.003(2)$ Å for C2 atom. The torsion angles of $174.9(2)^\circ$ for the atoms C11-C12-C13-C14 indicate that the propenone chain is oriented in a +anti-periplanar conformation. The methoxy groups are substituted at the C16 and C19 positions of the phenyl ring.

Table 1. Crystal data and structure refinement details for the compound.

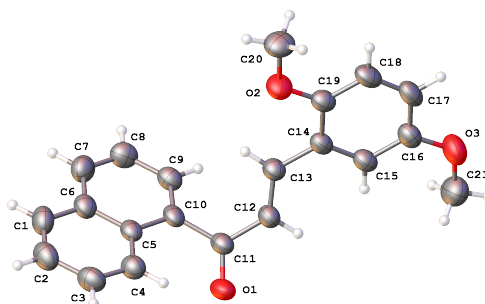
| | |
|--|---|
| Empirical formula | C ₂₁ H ₁₈ O ₃ |
| Formula weight | 318.35 |
| Temperature (K) | 293(2) |
| Crystal system | Triclinic |
| Space group | P-1 |
| a (Å) | 7.7705(4) |
| b (Å) | 10.2634(6) |
| c (Å) | 11.2487(6) |
| α (°) | 79.655(5) |
| β (°) | 81.500(5) |
| γ (°) | 68.039(5) |
| Volume (Å ³) | 815.28(9) |
| Z | 2 |
| ρ _{calc} (g/cm ³) | 1.297 |
| μ (mm ⁻¹) | 0.086 |
| F(000) | 336.0 |
| Crystal size (mm ³) | 0.310 × 0.240 × 0.230 |
| Radiation | MoKα (λ = 0.71073) |
| 2θ range for data collection (°) | 4.318 to 52.728 |
| Index ranges | -9 ≤ h ≤ 9, -11 ≤ k ≤ 12, -14 ≤ l ≤ 14 |
| Reflections collected | 9126 |
| Independent reflections | 3302 [R _{int} = 0.0466, R _{sigma} = 0.0528] |
| Data/restraints/parameters | 3302/0/219 |
| Goodness-of-fit on F ² | 1.050 |
| Final R indexes [I ≥ 2σ (I)] | R ₁ = 0.0568, wR ₂ = 0.1350 |
| Final R indexes [all data] | R ₁ = 0.0938, wR ₂ = 0.1667 |
| Largest diff. peak/hole (e Å ⁻³) | 0.17/-0.20 |

Table 2. Comparison of bond lengths of selected non-hydrogen atoms.

| Atoms | Length (Å) | | Atoms | Length (Å) | |
|--------|------------|-------|---------|------------|-------|
| | XRD | DFT | | XRD | DFT |
| O1-C11 | 1.229(2) | 1.198 | C10-C11 | 1.500(3) | 1.508 |
| O2-C19 | 1.366(2) | 1.353 | C12-C13 | 1.330(3) | 1.328 |
| O3-C16 | 1.379(3) | 1.352 | C14-C15 | 1.395(3) | 1.392 |
| C4-C5 | 1.419(3) | 1.423 | C14-C19 | 1.394(3) | 1.393 |
| C7-C8 | 1.359(3) | 1.359 | C16-C17 | 1.378(3) | 1.386 |
| C9-C10 | 1.365(3) | 1.362 | C18-C19 | 1.388(3) | 1.388 |

Table 3. Comparison of bond angles of selected non-hydrogen atoms.

| Atoms | Angle (°) | | Atoms | Angle (°) | |
|------------|------------|-------|-------------|------------|-------|
| | XRD | DFT | | XRD | DFT |
| C19-O2-C20 | 118.16(17) | 119.7 | O1-C11-C10 | 120.26(18) | 120.4 |
| C2-C1-C6 | 121.0(2) | 120.9 | O1-C11-C12 | 119.26(19) | 119.2 |
| C1-C2-C3 | 120.5(2) | 120.3 | C10-C11-C12 | 120.46(18) | 120.3 |
| C4-C5-C6 | 118.29(19) | 118.3 | C11-C12-C13 | 125.4(2) | 125.2 |
| C1-C6-C5 | 119.1(2) | 119.4 | O2-C19-C18 | 124.29(19) | 124.3 |
| C9-C10-C11 | 119.10(19) | 119.3 | C14-C19-C18 | 119.8(2) | 119.4 |

**Figure 3.** The ORTEP of the molecule with thermal ellipsoids drawn at 50% probability.

The bond length of C11-O1 is 1.228(3) Å, which shows similar bond length with the other chalcone derivatives [19]. The torsion angles of 177.8(2)° and 179.7(2)° for the atoms C20-O2-C19-C14 and C14-C15-C16-O3 showed that they were oriented in +anti-periplanar conformations, respectively. The structure exhibits C-H...O intermolecular and intramolecular interaction. The hydrogen bond interaction is listed in Table 5. The packing of the molecules when viewed down a axis is shown in Figure 4. Further, the structure is stabilized by π-π interactions. Cg is the centroid of the ring C14-C15-C16-C17-C18-C19 with Cg...Cg distance of 4.080(14) Å, and perpendicular distance of Cg on itself is -3.5138(9) Å with a

slippage value of 2.073 Å. The symmetry code for the Cg...Cg interaction is 1-x, -y, 2-z. The π...π interaction is shown in Figure 5.

3.2. Hirshfeld surface analysis

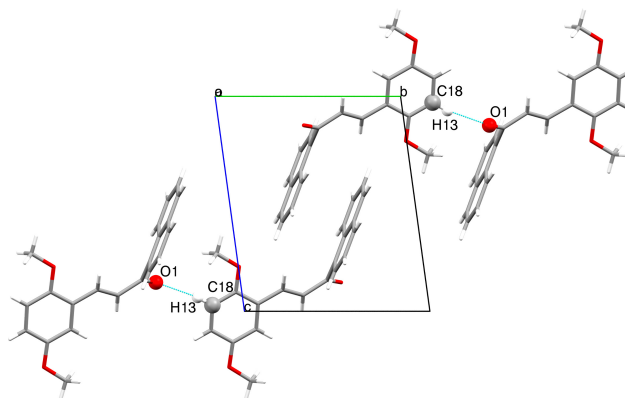
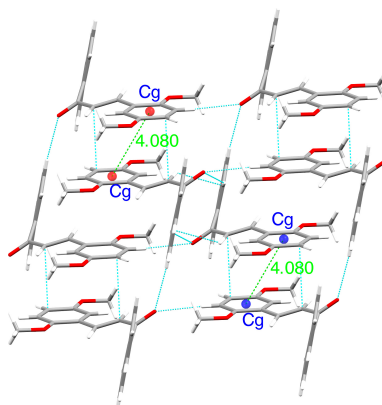
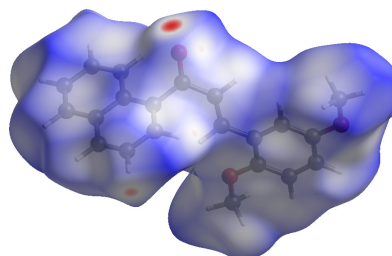
Hirshfeld surface analysis is used to study the interconnectivity of the molecules. It uses 'Stockholder partitioning' scheme to define the atoms in a molecule. Spackman and Byron introduced a new method to partition the electron densities into fragment contributions based on the Hirshfeld Stockholder partitioning scheme [20,21].

Table 4. Comparison of torsion angles of selected non-hydrogen atoms.

| Atoms | Angle (°) | | Atoms | Angle (°) | |
|----------------|------------|--------|-----------------|------------|--------|
| | XRD | DFT | | XRD | DFT |
| C20-O2-C19-C14 | 177.80(18) | -178.4 | C7-C8-C9-C10 | 1.6(3) | 1.2 |
| C20-O2-C19-C18 | -1.0(3) | 0.9 | C11-C12-C13-C14 | 174.87(19) | 175.1 |
| C2-C1-C6-C7 | -179.5(2) | -179.9 | C13-C14-C15-C16 | 179.52(19) | -179.4 |
| C4-C5-C6-C7 | 178.15(18) | -179.8 | C14-C15-C16-O3 | 179.73(18) | 179.4 |
| C1-C6-C7-C8 | 179.5(2) | 179.0 | C16-C17-C18-C19 | -0.1(3) | 0.04 |
| C5-C6-C7-C8 | -0.8(3) | -0.7 | C17-C18-C19-O2 | 179.04(19) | -179.9 |

Table 5. Hydrogen bond interactions.

| D-H...A | D-H (Å) | H...A (Å) | D-A (Å) | ∠D-H...A (°) |
|---------------------------|---------|-----------|----------|--------------|
| C18-H13...O1 ⁱ | 0.93 | 2.53 | 3.453(3) | 172 |

ⁱ 1-x, -y, 2-z.**Figure 4.** Packing of the molecules viewed along *a* axis.**Figure 5.** The molecules showing π - π interactions in the crystal structure.**Figure 6.** Hirshfeld surface mapped with normalized contact distance d_{norm} .

The resulting surfaces are called Hirshfeld surfaces. They help to identify the intermolecular interactions that are responsible for the connectivity of the molecules in the crystal structure.

Hirshfeld surface study is a powerful tool which is used to visualize the intermolecular interactions by a 3-D color coding system. This can further be resolved into 2D fingerprint plots,

which quantitatively summarize the nature and type of intermolecular contacts in the crystal [22]. The surfaces generated using d_{norm} function are illustrated for a clear visualization of the molecules. The high resolution Hirshfeld surfaces are mapped with the function d_{norm} , where d_{norm} is the normalized contact distance which is surface property and is given by

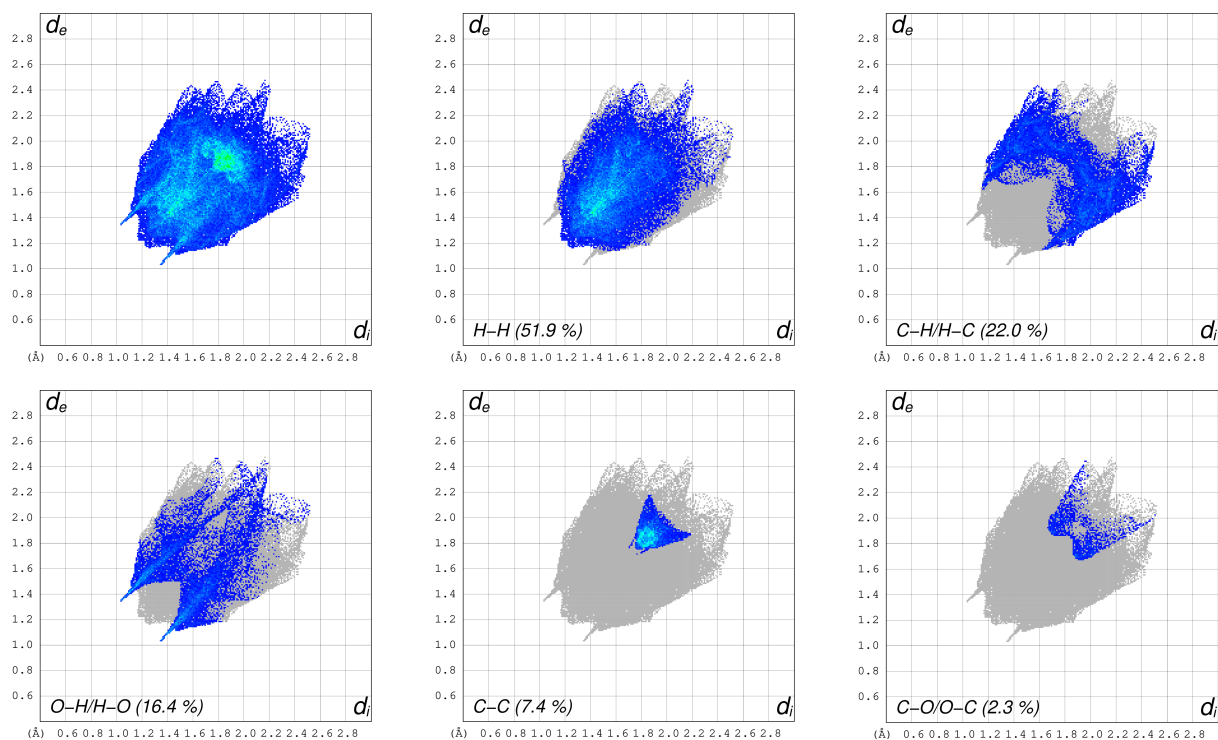


Figure 7. Fingerprint plot of the individual contacts to the total Hirshfeld surface.

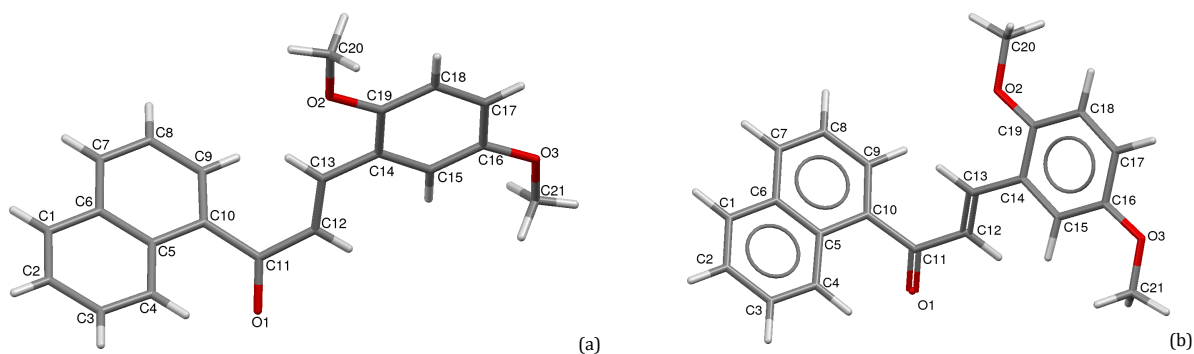


Figure 8. Comparison of the experimental structure (a) with optimized structure (b) of the title compound.

$$d_{\text{norm}} = \frac{d_i - r_i^{\text{vdw}}}{r_i^{\text{vdw}}} + \frac{d_e - r_e^{\text{vdw}}}{r_e^{\text{vdw}}} \quad (1)$$

where d_i and d_e are the distances from the nearest nucleus inside and outside of the molecule from the Hirshfeld surface, respectively, and r_i^{vdw} and r_e^{vdw} are the van der Waals radii.

Hirshfeld surface and 2D fingerprint plots were generated using CrystalExplorer17 [23]. The Hirshfeld surface mapped over d_{norm} is shown in Figure 6. The bright red spot on the d_{norm} surface is due to the presence of intermolecular C-H...O interactions. The fingerprint plots show the various contributions to the total Hirshfeld surface area with individual contacts H...H (51.9%), C...H/H...C (22.0%), O...H/H...O (16.4%), C...C (7.4%), C...O/O...C (2.3%) (Figure 7). The major contribution is from H...H contacts and the least is from O...H contacts.

3.3. Density functional theory (DFT)

DFT is a computational approach to know the electronic properties of the molecule. The molecular structure is optimized in the gas phase using Gamess software [24] with

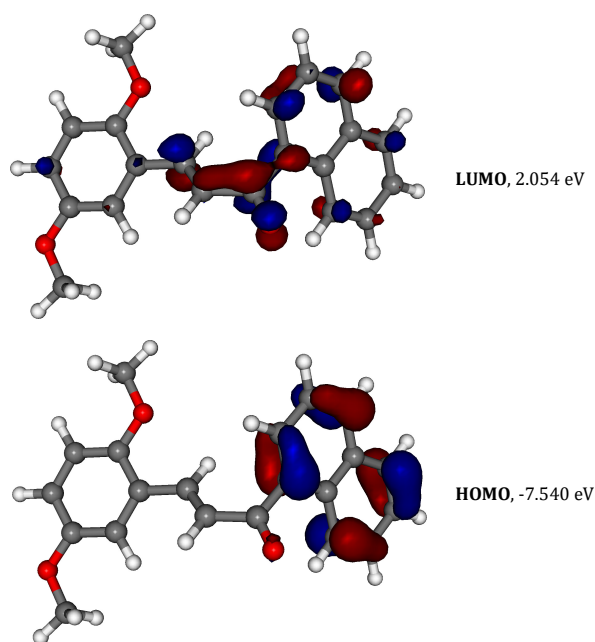
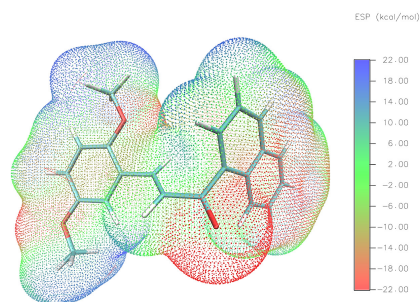
B3LYP functional with the 6-31G(d, p) basis set. Comparisons of bond lengths, bond angles, and torsion angles of optimized structure with the X-ray crystallographic structure are drawn (Tables 3-4). In addition, the experimental and theoretical structures are shown in Figure 8. The small deviation observed can be ascribed to the gas phase calculation.

3.4. Frontier molecular orbitals

The frontier molecular orbitals Highest Occupied Molecular Orbital (HOMO) and Lowest Unoccupied Molecular Orbital (LUMO) are used to predict the energy level, kinetic stability, and chemical reactivity of a molecule. The energy of HOMO and LUMO gives the values of electron affinity and ionization potential of the molecule, respectively. The energy difference between the HOMO and LUMO is termed as energy gap. The DFT calculations were performed with B3LYP/6-31 G (d, p) basis set. The energy gap predicts the kinetic stability and chemical reactivity of the molecule [25]. The energy gap for the molecule is found to be 5.486 eV. The Energy level of frontier molecular orbitals is shown in Figure 9.

Table 6. Molecular descriptors and their energies.

| Descriptor | Value (eV) |
|-------------------------------|------------|
| HOMO | -7.540 |
| LUMO | 2.054 |
| Energy gap (ΔE) | 5.486 |
| Ionization potential (I) | 7.540 |
| Electron affinity (E) | 2.054 |
| Chemical potential (μ) | -4.797 |
| Electronegativity (χ) | 4.797 |
| Global hardness (σ) | 0.364 |
| Global softness (η) | 2.743 |
| Electrophilicity (ω) | 4.194 |

**Figure 9.** Energy levels of frontier molecular orbitals.**Figure 10.** The MEP plot of the title compound.

Electronegativity, softness, hardness, chemical potential, and other chemical properties are derived from the energies of HOMO and LUMO.

The electronegativity (χ) is the average of the ionization potential and electron affinity of the molecule. Its measure of the tendency of attracting electrons. The idea of hardness and softness of the molecule was introduced by Pearson *et al.* [26]. Molecules with small size, high electronegativity are referred as hard molecules, while molecules large in size and low electronegativity are known as soft molecules [27]. The molecular properties are calculated using the formulae, $I = -E_{\text{HOMO}}$, $A = E_{\text{LUMO}}$, $\chi = 1/2(I + A)$, $\mu = -\chi$, $\eta = \Delta E/2$, $\sigma = 1/\eta$, and $\omega = \mu^2/2\eta$. The calculated values of molecular descriptors are listed in Table 6.

3.5. Molecular electrostatic potential (MEP)

The molecular behavior can be understood by generating the electrostatic potential surface around the molecule. The MEP surface is defined as, at any point $r(x, y, z)$ in the vicinity of a molecule, the potential energy is generated by the nuclei, electrons, and molecules and a proton [28]. At any point r , $V(r)$ is given by

$$V(r) = Z_A / (R_A - r) \quad (2)$$

where $V(r)$ is the potential energy at r , Z_A is the charge on the nucleus. The molecular electrostatic potential maps were generated using Multiwfn software [29] with the B3LYP/631-G(d, p) basis set. The MEP surface is shown in Figure 10.

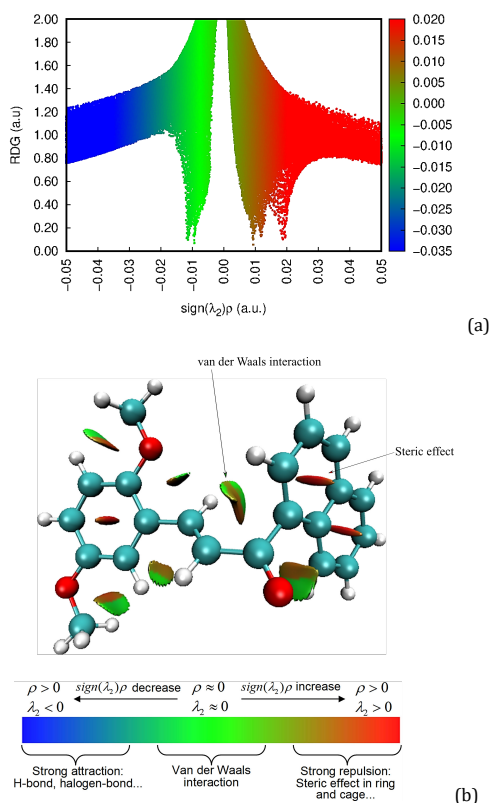


Figure 11. The 2D scattered plot and RDG isosurface of the title molecule.

The MEP map is useful to understand the chemical reactive sites in the molecule. The red and blue colored regions on the MEP indicate of electrophilic sites and nucleophilic sites, respectively. Figure 10 shows that the electrophilic sites are around the oxygen atoms while the nucleophilic sites are concentrated over hydrogen atoms.

3.6. Reduced density gradient (RDG)

Reduced density gradient $R(r)$ is a topological method employed to visualize the non-covalent interactions (NCIs) like hydrogen bond interactions, van der Waals interaction and steric effects in a molecule. It is a function of electron density $\rho(r)$ and its gradient. The equation for $R(r)$ is given by,

$$R(r) = \frac{1}{2(3\pi^2)^{1/3}} \frac{|\nabla\rho(r)|}{\rho(r)^{4/3}} \quad (3)$$

RDG is a dimensionless quantity of the inhomogeneity of the density at a point of space r [30]. To analyze the reduced density gradient, DFT calculations were performed using *Gamess* software [24] with B3LYP/6-31G(d,p) basis set. The RDG plot was generated by Multiwfn [29] and *VMD* [31] software. The RDG was analyzed by plotting $R(r)$ against the product of the density and the sign of the second eigenvalue of the electron density of Hessian matrix ($\text{sign}(\lambda_2)\rho(r)$). The 2D scattered plot and the corresponding RDG isosurface of the title molecule is shown in Figure 11. The region at the center of the ring with red color shows a strong steric effect, and the green color indicates the van der Waals interaction (Figure 11b).

The sign of λ_2 is used to distinguish between the regions of strong attraction ($\lambda_2 < 0$) and strong repulsion ($\lambda_2 > 0$). Figure 11b shows the van der Waals interaction between H14 of the naphthalene ring and O3 atom. A strong hydrogen bond is absent in the molecule. The right peak (Figure 11a) with red color corresponds to the steric repulsion at the center of the

naphthalene ring with the $\text{sign}(\lambda_2)\rho(r)$ value in the range 0.01-0.02 a.u. The van der Waals interactions and steric clash are represented by the isosurface value 0.6.

4. Conclusion

The synthesized compound crystallizes in the triclinic crystal system with the space group P-1. The structure was reinforced by C-H...O interaction. The Hirshfeld surface analysis confirmed the presence of intermolecular interactions. The fingerprint plots show the major contribution to the total molecular surface was from H...H contacts (51%). The calculated energy difference between the frontier molecular orbitals gives an energy gap of 5.486 eV which shows the kinetic stability of the molecule. The MEP map shows the chemical reactive sites of the molecule are around the oxygen (electronegative) and hydrogen (electropositive) atoms. The RDG analysis revealed the presence of van der Waals interactions and steric clashes in the molecule.

Acknowledgments

Prabhuswamy Akhileshwari thanks Department of Science and Technology - Karnataka Science and Technology Promotion Society (DST-KSTePS), Government of Karnataka, for providing the fellowship.

Supporting information

CCDC-2054693 contains the supplementary crystallographic data for this paper. These data can be obtained free of charge via <https://www.ccdc.cam.ac.uk/structures/> or by e-mailing data_request@ccdc.cam.ac.uk or by contacting The Cambridge Crystallographic Data Centre, 12 Union Road, Cambridge CB2 1EZ, UK; fax: +44(0)1223-336033.

Disclosure statement 

Conflict of interests: The authors declare that they have no conflict of interest.

Author contributions: All authors contributed equally to this work.

Ethical approval: All ethical guidelines have been adhered.

Sample availability: Samples of the compounds are available from the author.

ORCID 

Madhu Kumar Dogganal Jayappa

 <https://orcid.org/0000-0002-9391-4252>

Prabhuswamy Akhileshwari

 <https://orcid.org/0000-0003-0716-3542>

Mandayam Anandalwar Sridhar

 <https://orcid.org/0000-0002-3065-3630>

Lohith Tumakuru Nagarajappa

 <https://orcid.org/0000-0003-1808-740X>

Shivegowda Nagaraju

 <https://orcid.org/0000-0001-6001-068X>

Subrayachar Raghavendra

 <https://orcid.org/0000-0002-9633-953X>

Manasa Dogganal Jayappa

 <https://orcid.org/0000-0002-6584-1922>

References

- Rammohan, A.; Reddy, J. S.; Sravya, G.; Rao, C. N.; Zyryanov, G. V. *Environ. Chem. Lett.* **2020**, *18* (2), 433–458.
- Budhiraja, A.; Kadian, K.; Kaur, M.; Aggarwal, V.; Garg, A.; Sapra, S.; Nepali, K.; Suri, O. P.; Dhar, K. L. *Med. Chem. Res.* **2011**, *21* (9), 2133–2140.
- Nishimura, R.; Tabata, K.; Arakawa, M.; Ito, Y.; Kimura, Y.; Akihisa, T.; Nagai, H.; Sakuma, A.; Kohno, H.; Suzuki, T. *Biol. Pharm. Bull.* **2007**, *30* (10), 1878–1883.
- Chen, J. J.; Cheng, M. J.; Shu, C. W.; Sung, P. J.; Lim, Y. P.; Cheng, L. Y.; Wang, S. L.; Chen, L. C. *Chem. Nat. Compd.* **2017**, *53* (4), 632–634.
- Song-San, S.; Watanabe, S.; Saito, T. *Phytochemistry* **1989**, *28* (6), 1776–1777.
- Lei, W.; Sun, M.; Luo, K. M.; Shui, X. R.; Sun, Y. M.; Tang, S. H. *Mol. Biol.* **2009**, *43* (6), 1008–1013.
- Fang, X.; Yang, B.; Cheng, Z.; Zhang, P.; Yang, M. *Res. Chem. Intermed.* **2013**, *40* (4), 1715–1725.
- Chavan, B. B.; Gadekar, A. S.; Mehta, P. P.; Vavhal, P. K.; Kolsure, A. K.; Chabukswar, A. R. *Asian. J. Bio. Phar. Sci.* **2016**, *6* (56), 1–7.
- Rahman, M. *Chem. Sci. J.* **2011**, *2* (1), CSJ-29, 1–16.
- Mobinikhaled, A.; Foroughifar, N.; Zendehtdel, M. *Synth. React. Inorg. Met. Org., Nano-Met. Chem.* **2007**, *37* (4), 225–228.
- Budhiraja, A.; Kadian, K.; Kaur, M.; Aggarwal, V.; Garg, A.; Sapra, S.; Nepali, K.; Suri, O. P.; Dhar, K. L. *Med. Chem. Res.* **2011**, *21* (9), 2133–2140.
- Kalirajan, R.; Sivakumar, S. U.; Jubie, S.; Gowramma, B.; Suresh, B. *Int. J. Chem. Tech. Res.* **2009**, *1* (1), 27–34.
- Madhu, K. D. J.; Jagadeesh, P. D.; Prakash, A. C.; Sana, S.; Chandrashekar, K. R. *Int. J. Adv. Res. Chem. Sci.* **2015**, *2* (7), 43–51.
- Rigaku, CrystalClear-SM Expert and CrystalStructure. Rigaku Corporation, Tokyo, Japan, 2011.
- Sheldrick, G. M. *Acta Cryst. A* **2007**, *64* (1), 112–122.
- Johnson, C. K. ORTEP-II: A FORTRAN Thermal-Ellipsoid Plot Program for Crystal Structure Illustrations; Office of Scientific and Technical Information (OSTI), Oak Ridge National Laboratory Report ORNL-5138, 1976.
- Macrae, C. F.; Sovago, I.; Cottrell, S. J.; Galek, P. T. A.; McCabe, P.; Pidcock, E.; Platings, M.; Shields, G. P.; Stevens, J. S.; Towler, M.; Wood, P. A. *J. Appl. Cryst.* **2020**, *53* (1), 226–235.
- Allen, F. H.; Kennard, O.; Watson, D. G.; Brammer, L.; Orpen, A. G.; Taylor, R. *J. Chem. Soc., Perkin Trans. 2* **1987**, *12*, S1–19.
- Pramodh, B.; Lokanath, N. K.; Naveen, S.; Naresh, P.; Ganguly, S.; Panda, J. *J. Mol. Struct.* **2018**, *1161*, 9–17.
- Spackman, M. A.; Byrom, P. G. *Chem. Phys. Lett.* **1997**, *267* (3–4), 215–220.
- Spackman, M. A.; Jayatilaka, D. *CrystEngComm* **2009**, *11* (1), 19–32.
- Kumara, K.; Jyothi, M.; Zabiulla; Shivalingegowda, N.; Khanum, S. A.; Krishnappagowda, L. N. *Chem. Data Collect.* **2017**, *9–10*, 152–163.
- Jayatilaka, D.; Wolff, S. K.; Grimwood, D. J.; McKinnon, J. J.; Spackman, M. A. *Acta Cryst. A* **2006**, *62* (a1), s90–s90.
- Schmidt, M. W.; Baldrige, K. K.; Boatz, J. A.; Elbert, S. T.; Gordon, M. S.; Jensen, J. H.; Koseki, S.; Matsunaga, N.; Nguyen, K. A.; Su, S.; Windus, T. L.; Dupuis, M.; Montgomery, J. A. *J. Comput. Chem.* **1993**, *14* (11), 1347–1363.
- Karupphasamy, P.; Kamalesh, T.; Anitha, K.; Abdul Kalam, S.; Senthil Pandian, M.; Ramasamy, P.; Verma, S.; Venugopal Rao, S. *Optical Mater.* **2018**, *84*, 475–489.
- Pearson, R. G. *J. Chem. Sci.* **2005**, *117* (5), 369–377.
- Aihara, J. *Theoret. Chim. Acta* **1999**, *102* (1–6), 134–138.
- Scrocco, E.; Tomasi, J. *Electronic Molecular Structure, Reactivity and Intermolecular Forces: An Euristic Interpretation by Means of Electrostatic Molecular Potentials*. In *Advances in Quantum Chemistry* Volume 11; Elsevier, 1978; pp 115–193.
- Lu, T.; Chen, F. *J. Comput. Chem.* **2011**, *33* (5), 580–592.
- Laplaza, R.; Peccati, F.; A. Boto, R.; Quan, C.; Carbone, A.; Piquemal, J.; Maday, Y.; Contreras-Garcia, J. *WIREs Comput. Mol. Sci.* **2020**, e1497, 1–18.
- Humphrey, W.; Dalke, A.; Schulten, K. *J. Mol. Graph.* **1996**, *14* (1), 33–38.



Copyright © 2021 by Authors. This work is published and licensed by Atlanta Publishing House LLC, Atlanta, GA, USA. The full terms of this license are available at <http://www.eurjchem.com/index.php/eurjchem/pages/view/terms> and incorporate the Creative Commons Attribution-Non Commercial (CC BY NC) (International, v4.0) License (<http://creativecommons.org/licenses/by-nc/4.0>). By accessing the work, you hereby accept the Terms. This is an open access article distributed under the terms and conditions of the CC BY NC License, which permits unrestricted non-commercial use, distribution, and reproduction in any medium, provided the original work is properly cited without any further permission from Atlanta Publishing House LLC (European Journal of Chemistry). No use, distribution or reproduction is permitted which does not comply with these terms. Permissions for commercial use of this work beyond the scope of the License (<http://www.eurjchem.com/index.php/eurjchem/pages/view/terms>) are administered by Atlanta Publishing House LLC (European Journal of Chemistry).